Jun Li, Elena A. Medina, Judith K. Stalick, Arthur W. Sleight* and M.A. Subramanian*

Structural studies of $CaAl_{12}O_{19}$, $SrAl_{12}O_{19}$, $La_{2/3+\delta}Al_{12-\delta}O_{19}$, and $CaAl_{10}NiTiO_{19}$ with the hibonite structure; indications of an unusual type of ferroelectricity

DOI 10.1515/znb-2015-0224
Received December 31, 2015; accepted January 10, 2016

Abstract: Various oxides with the hibonite structure were synthesized and structurally analyzed using powder neutron diffraction. The structure of $CaAl_{12}O_{19}$ at 298 and 11 K shows dipoles that are apparently too dilute to order unless subjected to a suitable electric field. Magnetoplumbites, such as $BaFe_{12}O_{19}$, are isostructural with hibonite. These compounds possess ferromagnetic properties, which combined with the electric dipoles may influence multiferroic behavior. Our $SrAl_{12}O_{19}$ sample showed two distinct hexagonal phases, a major phase with the normal hibonite structure and a minor phase having a closely related structure. Our sample of the defect hibonite phase $La_{2/3+\delta}Al_{12-\delta}O_{19}$ shows a distinctly higher δ value (0.25) vs. that reported (~0.15) for samples made from the melt. Finally, we used to advantage the negative scattering length of Ti to determine the site occupancies of Ni and Ti in $CaAl_{10}NiTiO_{19}$.

Keywords: crystal structure; ferroelectricity; hibonite; neutron diffraction; oxides.

Dedicated to: Professor Wolfgang Jeitschko on the occasion of his 80th birthday.

1 Introduction

The mineral hibonite only rarely occurs naturally on our planet, but it is frequently found in chondritic meteorites that impact our planet [1, 2]. The ideal hibonite formula is $CaAl_{12}O_{19}$, but minerals occur with Si, Ti, V, Cr, Fe, Mn, Zn, and Mg substituting for Al [1–3]. The compounds $SrAl_{12}O_{19}$, $PbAl_{12}O_{19}$, $SrGa_{12}O_{19}$, and $BaGa_{12}O_{19}$ with the hibonite structure have been synthesized [4, 5]. The hibonite structure is also the structure found for magnetoplumbites such as $BaFe_{12}O_{19}$ [6].

The hibonite structure (Fig. 1) is hexagonal and contains five different sites for Al. The Al coordination number (CN) is 6 for three of these sites and 4 for one of these sites. The 5th site (Al2) ideally has trigonal bipyramidal (TBP) symmetry with very long apical distances. However, the most recent diffraction studies conclude that the cation at the TBP site is always displaced toward one of the apical O atoms giving it a CN of 4 [4, 7, 8]. This has been confirmed by ^{27}Al NMR studies in the case of $SrAl_{12}O_{19}$ [9]. The three Al sites with CN 6 are described as octahedral but none have ideal octahedral symmetry, which cannot occur strictly in hexagonal symmetry. The Al (Al1) atom at the origin (an inversion center) has ideal trigonal antiprismatic symmetry. Two AlO_6 octahedra share a common face utilizing the Al4 site. The AlO_6 octahedra based on the Al5 site form a sheet perpendicular to the *c* axis. Each of these octahedra shares edges with four other AlO_6 octahedra. These sheets together with the tetrahedral Al atoms of the Al3 site form a slab that occurs in the spinel and *β*-alumina structures. Reported bond valence sum (BVS) calculations for $CaAl_{12}O_{19}$ have shown that Al at the tetrahedral (Al3) site is underbonded [10], and we find that the Ca site and Al2 site are also underbonded and that the Al1 site is overbonded.

$CaAl_{12}O_{19}$ melts incongruently at 1850 °C [11]. However, there are many reports of growing large single crystals of substituted hibonite compositions from the melt [4, 5, 12–16]. These include $AAl_{12}O_{19}$ (*A* = Ca, Sr, Pb) and $LnAl_{11}MO_{19}$ compositions where *Ln* is La, Pr, Nd, Sm, or Eu and *M* is Mg, Mn, Fe, Co, Ni, or Cu. Several characteristics of hibonite compositions suggest that they are generally not thermodynamically stable at lower temperatures. One of these is that all successful $CaAl_{12}O_{19}$ syntheses require a temperature of at least 1300 °C, and hibonite mineral

***Corresponding authors: Arthur W. Sleight and M.A. Subramanian,** Department of Chemistry, Oregon State University, Corvallis, OR 97331, USA, e-mail: arthur.sleight@oregonstate.edu (A.W. Sleight), Mas.Subramanian@oregonstate.edu (M.A. Subramanian)
Jun Li and Elena A. Medina: Department of Chemistry, Oregon State University, Corvallis, OR 97331, USA
Judith K. Stalick: NIST Center for Neutron Research, National Institute of Standards and Technology, 100 Bureau Drive, Gaithersburg, MD 20899, USA

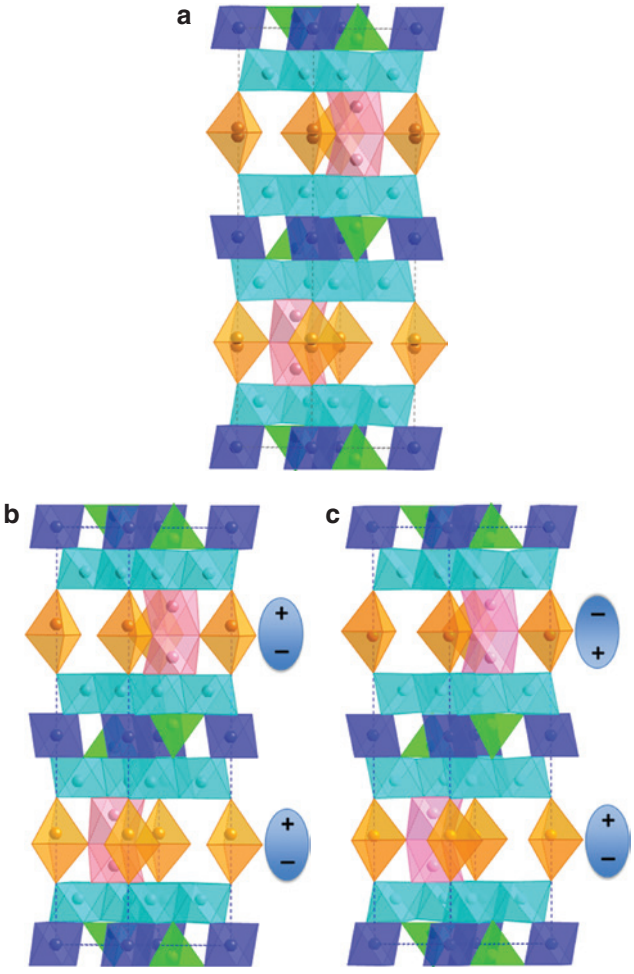

Fig. 1: The Al-O framework of the hibonite structure with the *c* axis vertical. Dark blue octahedron at the origin with Al1. The pink unit with Al4 are face-sharing octahedra. Turquoise octahedra of Al5 forming an edge sharing sheet. Green tetrahedra with Al3. The orange trigonal bipyramidal units with Al2. (a) The paraelectric structure ($P6_3/mmc$) with random displacements along the *c* axis. (b) Ordered dipoles in the ferroelectric structure ($P6_3mc$). (c) Ordered dipoles in the antiferroelectric structure ($P\bar{3}m1$).

samples apparently have been formed at very high temperatures. Another factor is the poor bond valence sums for several atoms in this structure. Still another factor pointing toward metastability is that there is always disorder at the Al2 site. The issue of metastability has been controversial, and the most recent evaluation of the situation concluded that present thermodynamic data cannot unambiguously determine whether or not hibonite is an entropy-stabilized phase, such as "FeO" [17].

The situation for magnetoplumbites such as $BaFe_{12}O_{19}$ is very similar to that of hibonites. Structural studies show that Fe in the TBP (Al2) site is actually displaced toward one of the apical O atoms in a disordered manner [7]. Mössbauer spectroscopic studies of ^{57}Fe as a function of temperature have indicated that the disorder is dynamic at room temperature and above, but well below room temperature these Fe atoms become trapped on one side of the basal plane triangle of O atoms [18]. There have apparently been no structural or ^{27}Al NMR studies for hibonites as a function of temperature. One aspect of our current study was to investigate the structure of $CaAl_{12}O_{19}$ as a function of temperature looking for evidence that the disorder of Al at the Al2 site might change with temperature.

Two studies have reported a hibonite structure in the La/Al/O system [12, 13]. A formula of $La_{2/3}Al_{12}O_{19}$ might be expected for this phase; however, the structural analyses have shown a significantly higher La content. Our sample examined by neutron diffraction shows even higher La content, and we discuss how the extra positive charge is compensated.

We have been interested in the optical properties of transition metal cations in TBP sites of oxides [19–21]. Our studies of the optical properties of hibonites containing partial transition metal substitutions for Al are presented elsewhere.

2 Experimental

Reactants were $CaCO_3$ (Spectrum, 99 %), $SrCO_3$ (Aldrich, 99.9 %), La_2O_3 (Alfa Aesar, 99.99 %), Al_2O_3 (Cerac, 99.99 %), NiO (Alfa Aesar, 99.998 %), and TiO_2 (Aldrich, 99.9 %). Appropriate quantities were ground together in an agate mortar and then pelleted. The pellets were then heated at a range of 1300–1500 °C in air several times with intermediate grinding. Ramp rates were 300 °C h^{-1}. The synthesis temperature was 1300 °C for $CaAl_{10}NiTiO_{19}$ and 1500 °C for $CaAl_{12}O_{19}$, $SrAl_{12}O_{19}$ and $La_{2/3+\delta}Al_{12-\delta}O_{19}$.

The products were characterized using a Rigaku Miniflex X-ray diffractometer with Cu K_α radiation and a graphite monochromator on the diffracted beam. Powder neutron diffraction data were collected on the 32-counter high-resolution diffractometer BT-1 at the Center for Neutron Research at the National Institute of Standards and Technology. A Cu(311) monochromator, yielding a wavelength of 1.5401(2) Å, was employed. Collimation of 15′ of arc was used before the monochromator, 20′ before the sample, and 7′ before the detectors. The samples were loaded into vanadium containers of 15.6 mm diameter and 50 mm length. Data were collected at room temperature over a 2θ range of 3–167°. In the case of $CaAl_{12}O_{19}$, data were also collected at 11 K. Structure refinements of XRD and neutron data by the Rietveld approach were carried out using GSAS-EXPGUI software [22, 23].

Refinement details may be found in cif files with the numbers CCDC 1454033-7 available at http://www.ccdc.cam.ac.uk/structures. The Rietveld fits are given in Supporting Information. Final structures were evaluated with difference Fourier maps. Anharmonic refinements used JANA2006 software [24].

Bond valence sums were calculated with the software EUTAX [25]. This software does not deal directly with the issues arising from split atoms. However, the bond valence sums produced can be corrected for the extra bonds produced utilizing the individual bond valencies, which are provided by the software.

3 Results

3.1 $CaAl_{12}O_{19}$

The structure of $CaAl_{12}O_{19}$ was refined from neutron diffraction data obtained at 11 K and 298 K. Three different structures were considered: paraelectric in space group $P6_3/mmc$ with disordered dipoles (Fig. 1a), ferroelectric in space group $P6_3mc$ (Fig. 1b), and antiferroelectric in space group $P\bar{3}m1$ (Fig. 1c). Good Rietveld fits (Fig. S1–S5; Supporting Information online) at both temperatures were obtained regardless of the space group assumed. No new peaks were observed in the low temperature diffraction pattern. For space groups $P6_3/mmc$ and $P6_3mc$ the only systematic absence is for *hhl* reflections when *l* is odd. There are no systematic absences in space group $P\bar{3}m1$, but intensities calculated for *hhl* relections with *l* odd are so weak (<0.1 % relative to the strongest peak) that they would not be observed even if present. The refinement in space group $P6_3mc$ did not converge due to correlations between atomic positions caused by the increased number of variables in the lower symmetry space group. The refinement converged in space group $P\bar{3}m1$. However, the fit did not improve significantly despite the six additional positional parameters. The structure was essentially unchanged except that now Al2 cations are ordered; there are no partially occupied sites. There was no improvement in the BVS values relative to the refinement in $P6_3/mmc$. Thus, we conclude that the structure is best described in $P6_3/mmc$ at 298 and 11 K (Table 1). Therefore, the dipoles are disordered at both 11 and 298 K. This does not preclude a model with considerable dipole ordering in chains along the *c* axis, but with a random polarity between adjacent chains. The lack of a second harmonic generation signal (SHG) at room temperature for $CaAl_{12}O_{19}$, $SrAl_{12}O_{19}$, and $PbAl_{12}O_{19}$ indicates all are centric at room temperature.

Table 1: Summary of $CaAl_{12}O_{19}$ rietveld refinement results.

	$T = 298$ K	$T = 11$ K
wR_p, %	4.72	3.90
R_p, %	3.65	3.12
χ^2	1.57	2.29
a, Å	5.5592(1)	5.5564(1)
c, Å	21.902(1)	21.867(1)
Ca: *x*	2/3	2/3
Ca: *z*	1/4	1/4
Ca: *U*, Å^2	0.015(1)	0.0091(6)
Al1: *x*	0	0
Al1: *z*	0	0
Al1: *U*, Å^2	0.0040(4)	0.0042(5)
Al2: *x*	0	0
Al2: *z*	0.2585(2)	0.2582(2)
Al2: *U*, Å^2	0.0018(9)	0.0010(9)
Al3: *x*	1/3	1/3
Al3: *z*	0.0286(1)	0.0283(1)
Al3: *U*, Å^2	0.0039(6)	0.0020(3)
Al4: *x*	1/3	1/3
Al4: *z*	0.1908(1)	0.1911(1)
Al4: *U*, Å^2	0.0051(8)	0.0010(9)
Al5: *x*	0.1688(2)	0.1680(1)
Al5: *z*	0.8909(1)	0.8909(4)
Al5: *U*, Å^2	0.0051(3)	0.0030(4)
O1: *x*	0	0
O1: *z*	0.1490(1)	0.1494(1)
O1: *U*, Å^2	0.0071(3)	0.0036(3)
O2: *x*	2/3	2/3
O2: *z*	0.0547(1)	0.0547(1)
O2: *U*, Å^2	0.0053(5)	0.0045(4)
O3: *x*	0.1807(1)	0.1815(1)
O3: *z*	1/4	1/4
O3: *U*, Å^2	0.0065(4)	0.0027(3)
O4: *x*	0.1547(1)	0.1550(1)
O4: *z*	0.0523(1)	0.0523(1)
O4: *U*, Å^2	0.0047(3)	0.0025(2)
O5: *x*	0.5034(1)	0.5034(1)
O5: *z*	0.1493(1)	0.1495(1)
O5: *U*, Å^2	0.0050(3)	0.0032(3)

This rules out ferroelectric ordering at room temperature but does not rule out antiferroelectric ordering. Our room temperature relative-permittivity data on pellets of these three compounds do not suggest enhanced polarizability (Table S1; Supporting Information online), but the concentration of dipoles is very low and they are only expected to be active in one direction.

Bond valence sum calculations for the refinement in space group $P6_3/mmc$ have shown low BVS values for Al3 in tetrahedral coordination and for Ca. These atoms would then be loosely bound and would be expected to show larger displacement parameters than the atoms showing BVS values close to those expected. The *U* value for Ca is much higher than the values obtained for Al or O

(Table 1). However, high displacement values for Al3 were not observed when using harmonic terms only. This is not surprising because an ellipsoid is not an appropriate shape for displacements of an atom at a tetrahedral site. Figure 2 shows the result of refining displacement factors incorporating anharmonic terms for Al3 and Al4. The site symmetry is the same for Al3 and Al4, but Al4 is not at a tetrahedral site. We see that in fact the shape obtained for Al3 is very anharmonic. The Zn atom in hexagonal ZnO is in the same type of site as Al3 in $CaAl_{12}O_{19}$. But in ZnO the BVS for Zn and O are normal, and applying anharmonic terms shown that an isotropic description of displacement factors is adequate [26].

3.2 $SrAl_{12}O_{19}$

Our neutron diffraction pattern for $SrAl_{12}O_{19}$ showed high angle shoulders for some, but not all, peaks (Fig. 3). Such shoulders can in some cases be modeled as anisotropic strain resulting from a sample with inhomogeneous composition. However, the shape of the peaks with shoulders in this case required a two-phase refinement. The cell dimensions of the main hexagonal phase and the minor hexagonal phase are $a = 5.5766$, $c = 22.143$ Å and $a = 5.5718$, $c = 22.012$ Å, respectively. The ratio of the two phases was about 4:1. The minor phase is contracted relative to the major phase by 0.6 % along c and only 0.09 % along a. Thus, the peak shoulders are caused almost exclusively by the contraction along c. Refinement of the primary phase indicated the presence $SrAl_{12}O_{19}$ with the hibonite structure (Table 2). Possibilities for the minor phase are suggested by findings in the Sr–Al–Mg–O system [27]. Single crystal studies in this system established both a β-alumina structure and a structure based on alternating layers of β-alumina and hibonite structures with ideal formulas of $SrMgAl_{10}O_{17}$ and $Sr_2MgAl_{22}O_{36}$, respectively. Without Mg and compensation with Sr vacancies, these formulae become $Sr_{0.5}Al_{11}O_{17}$ and $Sr_{1.5}Al_{23}O_{36}$. Both of these were evaluated as possible minor phases in our sample with the conclusion being that both structures gave an equivalently good result.

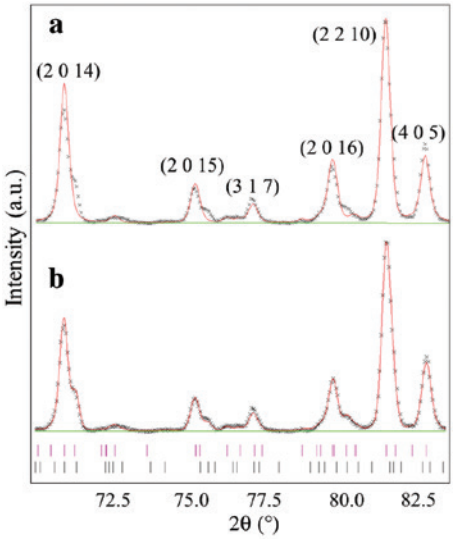

Fig. 3: A section of the neutron diffraction pattern for $SrAl_{12}O_{19}$. High angle shoulders occur on some, but not all, peaks. These shoulders are caused by a second hexagonal phase that is structurally related to that of hibonite. These shoulders are mainly caused by shortening of the c cell edge in the minor hexagonal phase. (a) Without the second hexagonal phase; (b) with the second hexagonal phase. Red markers for primary phase; black markers for minor phase.

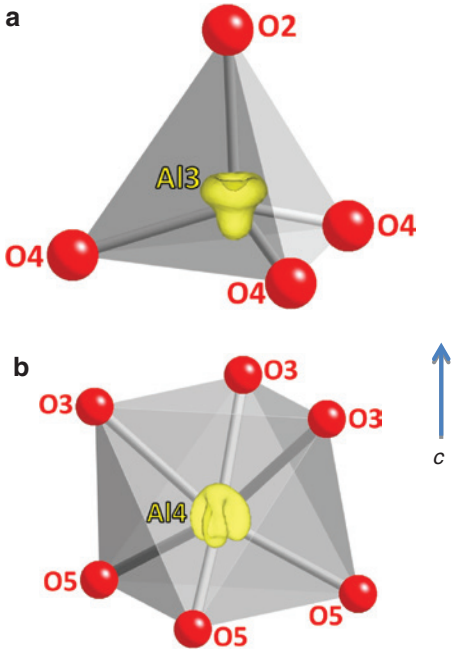

Fig. 2: Shapes of anharmonic displacements for Al at (a) the Al3 site and (b) the Al4 site, both in *4f 3m*. For the Al3 site there is major anharmonicity along the c axis, and minor anharmonicity perpendicular to c. For the Al4 site there is minor anharmonicity along c with more significant anharmonicity perpendicular to c.

3.3 $La_{2/3+\delta}Al_{12-\delta}O_{19}$

Refinement of our neutron diffraction data on the hibonite structure in the La/Al/O system gave results (Tables 3 and 4) similar to those obtained from two different single crystal XRD studies reported in 1984

Table 2: Summary of $SrAl_{12}O_{19}$ structure results (a = 5.5766 Å, c = 22.143 Å).

Atom	Wyckoff site	x[a]	z	U_{iso} (Å^2)
Sr	2*d*	2/3	1/4	0.010(1)
Al1	2*a*	0	0	0.003(1)
Al2	4*e*	0	0.2644(4)	0.009 (3)
Al3	4*f*	1/3	0.0268(3)	0.001(1)
Al4	4*f*	1/3	0.1883(3)	0.008(1)
Al5	12*k*	0.1694(4)	0.8922(1)	0.0077(5)
O1	4*e*	0	0.1485(2)	0.0002(7)
O2	4*f*	2/3	0.0556(2)	0.0015(6)
O3	6*h*	0.1828(4)	1/4	0.022(1)
O4	12*k*	0.1552(2)	0.0515(1)	0.0058(4)
O5	12*k*	0.5022(4)	0.1481(1)	0.0070(3)

[a]$y = 2x$.

Table 3: Summary of $La_{2/3+\delta}Al_{12-\delta}O_{19}$ structure results.

Atom	x[a]	z	U_{iso} (Å^2)	Occupancy[b]	Occupancy[c]
La1	2/3	1/4	0.005(1)	0.63(3)	0.64
La2	0.720(3)	1/4	0.005(1)	0.28(1)[d]	0.28
Al1	0	0	0.010(1)	1.0	1.016
Al2	0	0.2378(3)	0.009(2)	0.99(1)[d]	1.006
Al3	1/3	0.0270(2)	0.0010(6)	1.0	1.016
Al4	1/3	0.1898(2)	0.003(1)	1.0	1.016
Al5	0.1673(3)	0.8923(2)	0.0036(5)	0.946(9)	0.961
O1	0	0.1492(1)	0.0058(7)	1.0	1.016
O2	2/3	0.0569(1)	0.0061(5)	1.0	1.016
O3	0.1818(2)	1/4	0.007(1)	0.965(8)	0.980
O4	0.1540(2)	0.0524(1)	0.0057(5)	0.965(6)	0.980
O5	0.5047(2)	0.1502(1)	0.0056(5)	1.0	1.016

[a]$y = 2x$; [b]based on $La_{0.91}Al_{11.66}O_{18.69}$; [c]rescaled to $La_{0.92}Al_{11.85}O_{19}$; [d]sum of the split site.

Table 4: Comparison of structural data for $La_{2/3+\delta}Al_{12-\delta}O_{19}$ phase.

	XRD1[a]	XRD2[b]	Neutron
a, Å	5.550	5.561(2)	5.5756(1)
c, Å	22.031	22.07(1)	22.046(1)
c/a	3.970	3.969	3.954
La1 occup. (1/3, 2/3, ¾)	0.55	0.49(2)	0.63(3)
La2 occup.[c] (x, 2x, ¾)	0.3	0.34(2)	0.28(1)
Total La	0.85	0.83(2)	0.91(3)
δ	0.18	0.16	0.25
x (La2)	0.717	0.718(7)	0.720(3)
Al5 occup.	0.95	0.92(2)	0.946(9)
Al2 occup.[c]	0.82	0.85(7)	0.99(1)[c]

[a]Ref. [13], standard deviations not reported; [b]ref. [14]; [c]sum of the split site.

[13, 14]. The approximate formula can be represented as $La_{2/3+\delta}Al_{12-\delta}O_{19}$ with the Al vacancies confined to Al sites in the edge sharing sheets. Based on the refined La content, the values of δ obtained from the two XRD single crystal studies are 0.16 and 0.18. Our refinement gives a δ value of 0.25. One can expect the value of δ to vary with synthesis conditions, which were different. The single crystals were prepared from the melt at temperatures higher than 1700 °C. Our polycrystalline powders were prepared at 1500 °C. The vacancies on La and Al5 sites cause general disorder in the structure, which impedes an accurate description of the structure. The disorder in the planes at the z = ¼ and ¾ includes disorder within the plane for La, disorder of Al2 displaced from the plane, and a partial occupancy for O3. In addition, our difference Fourier map shows a peak just above and below the planes at x = 0.18, y = 0.36 with an intensity of about 6 % of an O atom. The disorder caused by the Al vacancies in the Al5 layer also causes apparent O vacancies at the O4 position, which is bonded to two Al5 atoms. Peaks in our difference Fourier map near the plane of Al5 atoms can also be attributed to the disorder at and near the Al5 plane. The refined composition yields a positive charge about 1 % too high for charge balance, but this is as close as could be expected based on the uncertainties of the occupation factors for several cation and anion sites.

Our results are compared to those of the two previous studies in Table 4. Due to common systematic errors, the c/a ratio is more reliable than the values of a and c themselves. This ratio is essentially the same for the two XRD studies, consistent with the fact that their value of δ is nearly the same. The c/a ratio for our sample is significantly smaller (Table 4), consistent with our higher La content. All three studies have found that an atomic fraction of 30–40 % of the La is displaced about 0.5 Å from the ideal site. We did not observe such displacements of La for $LaAl_{11}NiO_{19}$ hibonite where there are no La vacancies. We conclude that the displacement of some La atoms from the ideal site is caused by adjacent La site vacancies.

3.4 $CaAl_{10}NiTiO_{19}$

We have prepared and structurally characterized many hibonite phases where Al has been partially substituted by various 3*d* transition elements. Most of this work is reported in a separate paper that focuses on the optical properties of these phases, which show promise as pigments. Here we present our structural results on one such substitution, $CaAl_{10}NiTiO_{19}$. Determination of the distribution of Ni and Ti on the five different Al sites is challenging because one cannot refine the occupancies of Al, Ni, and Ti on one site even if one constrains the total site occupancies to be 100 % and constrains the overall stoichiometry

Table 5: Site occupations in $CaAl_{10}MTiO_{19}$ (M = Ni and Mg) samples.

Site	M = Ni[a]	M = Mg[b]
$M$1: trigonal antiprism	Ni: 0.06(1)	
$M$2: "trigonal bipyramid"	Ti: 0.112(5); Ni: 0.02[c]	Ti: 0.130(3)
$M$3: tetrahedral	Ni: 0.245(5)	Mg: 0.46(1)
$M$4: face-shared octahedra	Ti: 0.44(1)	Ti: 0.403(3)
$M$5: edge-shared octahedra	Ni: 0.073(4)	

[a]This work; refined composition: $CaAl_{10.02}Ni_{0.98}Ti_{1.00}O_{19}$; [b]Ref. [56]; refined composition with amounts of Mg and Ti constrained to be equal: $CaAl_{9.96}Mg_{0.98}Ti_{0.98}O_{19}$; [c]Ni fixed at value found for $LaAl_{11}NiO_{19}$ and $Ca_{0.5}La_{0.5}Al_{11.5}Ni_{0.5}O_{19}$.

of the compound. An unconstrained refinement of the three elements would require additional information, such as XRD data. One can, however, take advantage of the fact that whereas the scattering lengths for Al and Ni are positive with a much higher value for Ni, the scattering length of Ti is negative. Our strategy was to first refine the structure of a $CaAl_{10}NiTiO_{19}$ composition using 100 % Al in all five Al sites. Assuming that the Ca and O sites are essentially fully occupied, the scale factor would be set and the total scattering powers at the five Al sites would be determined. If the refined Al occupancy at a given site decreased, there must be Ti on that site with this assumption. If the refined Al occupancy on a given site increased above 100 %, there must be Ni on that site. The possibility that some Ni and Ti are both substituting on the same site is at first ignored except in the case of the TBP site where we fixed the Ni occupancy to the value we found for $LaAl_{11}NiO_{19}$ and $Ca_{0.5}La_{0.5}Al_{11.5}Ni_{0.5}O_{19}$. Next the sites with decreased scattering power were refined as a mixture of Al and Ti, and the sites with increased scattering power are refined as a mixture Al and Ni. The results of this refinement are presented in Table 5. The composition obtained from this refinement is $CaAl_{10.02}Ni_{0.98}Ti_{1.00}O_{19}$, which is very close to a nominal $CaAl_{10}NiTiO_{19}$ composition. We see that Ni is showing a strong preference for the tetrahedral site (Al3), and that Ti is showing a strong preference for the site with face-sharing octahedra (Al4). Significant Ti substitution also occurs at the Al2 (TBP) site. The results indicate some Ni on the Al1 and Al5 sites, and there could possibly be a very small amount of Ni on the Al4 site that is dominated by Ti substitution.

4 Discussion

A common feature of all simple $AM_{12}O_{19}$ compounds (A^{2+} = Pb, Ca, Sr, or Ba; M^{3+} = Al, Ga, or Fe) with the hibonite structure is that the M cations at both the tetrahedral site ($M$3) and the trigonal bipyramidal site ($M$2) are severely underbonded (Table 6). In some structures, such as the perovskite structure, such a poor bonding situation can be relieved by a distortion to a structure with lower symmetry. This option apparently is not available to the hibonite structure because no such distortions have ever been observed. A partial solution to this problem is to introduce larger cations into the structure that will be located mainly on the tetrahedral and/or the TBP sites. Examples are $LaAl_{11}NiO_{19}$ and $CaAl_{10}NiTiO_{19}$. Such substitutions also lower the required synthesis temperature.

The failure of the hibonite structure to adjust in a way that would give good BVS values at the $M$2 and $M$3 sites was explored by modeling with DLS software [28]. The results are given in Table 7. In one example, we see that obtaining a good BVS for tetrahedral Al2 can be obtained with small variations of a, c, and positional parameters. However, this is at a cost of changes in other BVS values

Table 6: Bond valence sums (BVS)[a] for $AM_{12}O_{19}$ (A = Ca, Sr, Ba; M = Al, Ga, Fe).

Site	PbAl [29]	CaAl This work	SrAl [6]	SrAl This work	SrGa [6, 30]	BaGa [7]	SrFe [6]	BaFe [8]
A	**1.97**	**1.49**	2.09	2.03	**1.67**	*2.39*	**1.54**	*2.27*
Al1: trigonal antiprism	*3.24*	*3.23*	*3.33*	*3.20*	3.16	3.14	3.12	3.13
Al2: "trigonal bipyramid"	**2.64**	**2.77**	**2.82**	**2.60**	**2.76**	**2.62**	**2.82**	**2.76**
Al3: tetrahedral	**2.63**	**2.68**	**2.58**	**2.61**	**2.69**	**2.62**	**2.76**	**2.78**
Al4: face-shared octahedra	2.89	3.00	3.16	2.89	2.96	2.83	3.05	2.99
Al5: edge-shared octahedra	3.09	3.09	3.09	3.02	3.09	3.05	*3.02*	2.97
O1: 3Al5, 1Al2[b]	1.96	2.02	1.94	**1.87**	2.01	1.95	1.92	**1.86**
O2: 1Al1, 3Al5	**1.86**	**1.85**	1.91	1.92	**1.88**	**1.84**	1.92	1.91
O3: 1Al2, 2Al4	**1.92**	**1.87**	**1.41**	**1.84**	**1.87**	1.93	**1.88**	1.96
O4: 1Al3, 1Al1, 2Al5	2.00	2.01	1.98	1.96	1.98	1.95	1.98	1.98
O5: 2Al5, 1Al4	2.00	1.99	2.40	2.02	2.03	2.05	2.00	2.03

[a]Underbonded values in bold; overbonded value in italics; [b]cations bonded to oxygen.

Table 7: Comparison of refined and modeled structure for $CaAl_{12}O_{19}$.

	Refined structure	DLS Al2: CN4	DLS Al2: CN5
a, Å	5.5592	5.5517	5.6320
c, Å	21.902	21.969	20.238
z, Al2	0.258	0.270	0.25
z, Al3	0.0286	0.0277	0.0399
z, Al4	0.1908	0.1911	0.1822
x, Al5	0.1686	0.1700	0.1705
z, Al5	0.1090	0.1091	0.1126
z, O1	0.1493	0.1493	0.1493
z, O2	0.0547	0.0534	0.0534
x, O3	0.1813	0.1779	0.1804
x, O4	0.1552	0.1550	0.1550
z, O4	0.0522	0.0523	0.0534
x, O5	0.5031	0.5030	0.5030
z, O5	0.1492	0.1493	0.1493
Al1–O4 × 6	**1.882**	**1.882**	**1.86**
Al2–O3 × 3	1.755	1.7673	1.78
Al2–O1	2.027	1.7694	2.04
Al2–O1′	2.384		2.04
Al2–Oave	**1.935**	**1.768**	**1.88**
Al3–O4 × 3	1.792	1.7985	1.78
Al3–O2	1.823	1.781	1.77
Al3–Oave	**1.800**	**1.794**	**1.78**
Al4–O5 × 3	1.871	1.873	1.82
Al4–O3 × 3	1.956	1.977	1.957
Al4–Oave	**1.914**	**1.925**	**1.887**
Al5–O5 × 2	1.809	1.803	1.773
Al5–O1	1.847	1.858	1.884
Al5–O2	1.984	1.991	1.970
Al5–O4 × 2	1.998	2.003	1.971
Al5–Oave	**1.906**	**1.910**	**1.890**
BVS Ca × 2	1.47	1.46	1.71
BVS Al1 × 2	3.24	3.21	3.42
BVS Al2 × 2	2.79	2.98	2.81
BVS Al3 × 4	2.65	2.72	2.94
BVS Al4 × 4	2.95	2.89	3.23
BVS Al5 × 12	3.10	3.07	3.31
BVS O1 × 4	2.14, 1.91	2.44, 1.78	2.18
BVS O2 × 4	1.85	1.90	1.99
BVS O3 ×× 6	1.85	1.78	1.78
BVS O4 × 12	2.00	1.98	2.12
BVS O5 × 12	2.00	2.01	2.30
Ave BVS |δ|[a]	**0.08**	**0.13**	**0.20**

[a]Average BVS uses absolute differences between BVS of Al with 3.0 and of O with 2.0. The multiplicities of atoms are incorporated. Values higher than ~0.1 suggest incorrect structure. Bold values indicate average bond length values.

that cause the overall BVS situation to degrade. The differences between the expected and observed BVS values were averaged based on the multiplicities of the atoms. Note that the BVS values based on the refined structure are close to those expected for the atoms with high multiplicity (Al5, O4, and O5). The failed attempt to obtain a good BVS for Al2 at an ideal TBP site (Table 7) demonstrates that the structure strongly resists such a variation.

The most significant factor resisting the adoption of a BVS close to 3.0 for Al2 appears to be the BVS for O1. As Al2 is displaced off the mirror plane (z = ¼), it moves toward one O1 increasing its BVS and away from another O1 decreasing its BVS. The O1 values for the refined structure are 2.14 and 1.91, both marginally acceptable values. The further displacement of Al2 to produce a good BVS for Al leads to BVS values of 2.44 and 1.78 for O1 (Table 7). These can be viewed as unacceptable deviations from 2.0. Thus, a displacement of Al2 large enough to produce a good BVS for Al does not occur.

4.1 Ferroelectric/multiferroic considerations

The situation in magnetoplumbites is the same as in hibonite compounds. Table 8 gives the displacements of the "TBP cations" from the ideal value of 0 0 ¼ in the center of the O triangle. The situation for hibonite/magnetoplumbite compounds is very much like the situation in $LiNbO_3$ and $LiTaO_3$. Switching polarity in an electric field causes in both cases a cation to move through the center of a triangle of O atoms. The displacements from the ideal paraelectric position are much greater for Li (~0.65 Å) than for the TBP cations in the hibonite/magnetoplumbite compounds. However, if net polarization for the dipoles is calculated based on formal charges, as is frequently practiced, the net polarization caused by the large displacements of Li and the smaller displacements for TBP cations is about the same. It is generally accepted that Li in the paraelectric states of $LiNbO_3$ and $LiTaO_3$ does not reside in the center of the O triangle, but is instead randomly distributed above and below this triangle [29]. The same situation apparently pertains to the "TBP cation" in hibonite/magnetoplumbite compounds.

Table 8: For the *M*2 (TBP) cation: displacement along *c* and bond valence sum (BVS).

Compound	Displacement (Å)[a]	BVS[b]
$CaAl_{12}O_{19}$	0.17	2.77, 2.77, 2.80
$SrAl_{12}O_{19}$	0.21	2.60, 2.60, 2.61
$PbAl_{12}O_{19}$ [30]	0.21	2.64, 2.64, 2.65
$SrGa_{12}O_{19}$ [31]	0.17	2.76, 2.76, 2.80
$BaGa_{12}O_{19}$ [7]	0.22	2.62, 2.62, 2.63
$SrFe_{12}O_{19}$ [6]	0.10	2.82, 2.82, 2.87
$BaFe_{12}O_{19}$ [8]	0.26	2.75, 2.76, 2.80

[a]Displacement of TBP cation from the ideal site (z = ¼) based on refinement of single crystal X-ray data; [b]bond valence sum for TBP cation at (1) ideal site, (2) reported site, and (3) site with four equal M–O bond lengths, respectively.

Table 8 also gives the bond valence sum for the TBP cation (*M*2) at various sites along the *c* axis. The first BVS value is for this cation placed at the ideal site ($z = ¼$). The second BVS value pertains to this cation placed according to the reported structure refinement. The final BVS value pushes this cation even further from the ideal site to a position where one of the apical distances is now equal to the three equatorial distances, a tetrahedral situation but with only one 3-fold axis. Note first that the BVS values are always much lower than the expected value of 3.0. Also note that the BVS does not change significantly as the TBP cation moves from the ideal TBP symmetry to a position where there would be four equal distances for tetrahedral coordination. We conclude from this that the TBP cation is loosely bound and that any barrier preventing its movement through the O triangle of the TBP unit is very small.

In situations where dipoles orient along a particular direction, simple electrostatic considerations favor ferroelectric chains as in Fig. 1b. This occurs in tetragonal $BaTiO_3$ and hexagonal $LiNbO_3$ where all the chains along the *c* axis are polarized in the same direction. However, simple electrostatic considerations would have half the chain dipoles ordered in one direction and half in another direction, as occurs in $PbZrO_3$ [32]. The triangular orientation of the chains in $YInO_3$ type structures causes a frustration, the result of which is that 1/3 of the chains are polarized up and 2/3 down. In some cases it has been demonstrated that the application of an electric field can cause such antiferroelectric or ferrielectric structures to become ferroelectric [33]. Thus even if the stable form of hibonite were antiferroelectric or ferrielectric, it would likely exhibit ferroelectric behavior when an electric field is applied along the *c* axis.

A very unusual aspect of the hibonite structure is the dilution of the dipoles. Only 1 out of 12 Al atoms participates, and the distance between such atoms is about 5.5 Å in the *ab* plane. The more important direction for dipole ordering is along the *c* axis where the distance between dipoles is about 11 Å. There are no O atoms that link the TBP units together. Ferroelectricity is well established in the hexagonal (again $P6_3/mmc$) oxides such as $YInO_3$, where also again there are no empty *d* levels close to the Fermi level, a condition frequently regarded as essential for ferroelectricity in oxides [34]. The dipoles in this $YInO_3$ structure are separated by only somewhat more than 3 Å, and they remain ordered up to very high temperatures (~1000 °C).

Mössbauer spectroscopic studies of ^{57}Fe in $BaFe_{12}O_{19}$ confirm that Fe at the TBP site is actually in tetrahedral coordination [18]. At higher temperatures it is jumping back and forth between sites on either side of the triangle of the TBP site. At temperatures well below room temperature the Fe atoms become trapped on one side of the triangle. The behavior of Al in hibonites is likely very much the same as that of Fe in $BaFe_{12}O_{19}$. The trapping of Fe at low temperatures does not infer that these displacements will necessarily produce an ordered arrangement of the dipoles.

The lack of dipole ordering in hibonite phases cannot be taken as evidence that they are not ferroelectrics. Amorphous materials with dipoles can develop ferroelectric properties by ordering of the dipoles in the presence of an electric field [35, 36]. The expected ferroelectric moment in hibonites is low due to the low concentration of dipoles and because the dipoles only occur along the *c* axis. However, in a dipole ordered structure, displacements of the loosely bound *M*3 cations can be expected to occur and contribute to the moment. Enhancement of a ferroelectric moment might also occur in $PbAl_{12}O_{19}$ due to the high polarizability of Pb^{2+}.

There are many reports of multiferroic behavior in magnetoplumbite phases [36–54]. The electrical conductivity, attributed to very small amounts of Fe^{2+} in such ferrites, is generally too high at room temperature to support ferroelectric behavior. However, the conductivity decreases with decreasing temperature allowing multiferroic behavior to be observed below room temperature. Some reports of multiferroic behavior at room temperature and above are most likely due to space charge polarization owing to electrical conductivity rather than actual ferroelectricity [55]. The polarization observed for the confirmed multiferroic magnetoplumbites is perpendicular to the *c* axis and thus cannot be related to the dipoles shown in Fig. 1. The observed polarization is instead attributed to mutually canted interacting spins producing the local electric polarization by a spin-orbit interaction [48]. It could be that spin-orbit interactions dominate for all the magnetoplumbite phases. Further studies on insulating single crystals are required to fully understand how the dipoles at the TBP sites in magnetoplumbites have an impact on their properties.

4.2 $CaAl_{10}NiTiO_{19}$

A very recent study described neutron diffraction refinements of $CaAl_{12}O_{19}$ samples with substitutions of Ti and Mg for Al [56]. Most of the compositions were purposely prepared under reducing conditions to produce some Ti^{3+}, but one composition, $CaAl_{9.96}Mg_{0.98}Ti_{0.98}O_{19}$, contained only Ti^{4+} and can thus be considered for comparison to our results for $CaAl_{10}NiTiO_{19}$ (Tables 5 and 9). These studies show a

Table 9: Comparison of interatomic distances for $CaAl_{12}O_{19}$, $CaAl_{10}NiTiO_{19}$, and $CaAl_{10}MgTiO_{19}$.

Distances (Å)	$CaAl_{12}O_{19}$	$CaAl_{11}NiTiO_{19}$	$CaAl_{11}MgTiO_{19}$ [56]
*M*1–O4 × 6	**1.8821**(8)	**1.8949**(15)	**1.888**
*M*2–O3 × 3	1.755(1)	1.7843(25)	1.776
*M*2–O1	2.027(5)	1.888(8)	1.924
*M*2–O1′	2.384(5)	2.580(8)	2.547
*M*2–Oave	**1.935**	**1.964**	**1.960**
*M*3–O4 × 3	1.792(1)	1.824(2)	1.825
*M*3–O2	1.823(3)	1.855(4)	1.849
*M*3–Oave	**1.800**	**1.832**	**1.831**
*M*4–*M*4	**2.595**(5)	**2.84**(7)	**2.80**
*M*4–O5 × 3	1.871(2)	1.84(1)	1.84
*M*4–O3 × 3	1.956(2)	2.06(6)	2.045
*M*4–Oave	**1.914**	**1.95**	**1.94**
*M*5–*M*5	2.748(3) × 2	2.786(5) × 2	2.770 × 2
*M*5–*M*5′	2.811(3) × 2	2.819(5) × 2	2.837 × 2
*M*5–*M*5ave	**2.780**	**2.803**	**2.804**
*M*5–O5 × 2	1.809(1)	1.855(2)	1.849
*M*5–O1	1.847(2)	1.879(3)	1.876
*M*5–O2	1.984(2)	1.957(3)	1.962
*M*5–O4 × 2	1.998(1)	1.980(2)	1.985
*M*5–Oave	**1.906**	**1.918**	**1.917**

Bold values indicate average bond length values.

strong preference of Mg and Ni for the tetrahedral site. This might be expected considering that Mg and Ni also prefer the tetrahedral sites in the spinels $MgAl_2O_4$ and $NiAl_2O_4$. Both studies also show a strong preference of Ti for the face sharing octahedral units, and both studies found about the same amount of Ti on the TBP *M*2 site. The two studies, however, differ with respect to the octahedral *M*1 and *M*5 sites. No substitution is reported for Al1 and Al5 in the study of $CaAl_{9.96}Mg_{0.98}Ti_{0.98}O_{19}$, but we find small but significant amounts of Ni on these two sites (Table 5). The very high scattering length of Ni (10.3 fm) vs. Al (3.449 fm), Mg (5.38 fm), and Ti (–3.438 fm) provides high accuracy for the amount of Ni on the *M*1 and *M*5 sites. A rather dramatic increase of the *M*2 cation distance from the triangle of the TBP unit has occurred with Ni and Mg substitution. This displacement, which was 0.17 Å in $CaAl_{12}O_{19}$, has become 0.31 Å in $CaAl_{10}MgTiO_{19}$ and 0.35 Å in $CaAl_{10}NiTiO_{19}$. Since Mg^{2+}, Ni^{3+}, and Ti^{4+} are all significantly larger than Al^{3+}, one might expect that bonding distances would increase as any of these cations replaces Al^{3+}. In fact, such increases are observed for all five Al sites in the case of $CaAl_{10}NiTiO_{19}$ (Table 5). In the case of $CaAl_{10}MgTiO_{19}$, the *M*–O distance at the *M*1 site has not increased significantly indicating any Mg substitution at that site is very small, in agreement with the report on $CaAl_{10}MgTiO_{19}$ [56]. However, in $CaAl_{10}MgTiO_{19}$ there is a significant increase in the average *M*5–O distance suggesting some Mg at this site, which was not reported [56]. It is not surprising that little or no Ti occupies the tetrahedral site because this is a rare site for Ti. Both studies have indicated that Ti also avoids the *M*1 octahedral site. Possibly, this is due to the overbonded situation at this site, which would worsen if Ti were introduced. Some Ti is expected to enter the *M*2 site because Ti^{4+} readily accepts TBP symmetry. There are strong cation-cation repulsive interactions across the edge-sharing octahedra in the case of the *M*5 cation and across face-sharing octahedra in the case of the *M*4 cations. One might then expect that the higher charge of Ti^{4+} would inhibit its substitution into the *M*4 and *M*5 sites. But in fact, Ti strongly prefers the *M*4 site to all other sites. Relative to the *M*5 site, there are two important factors. One is that the *M*4–*M*4 distance across the shared face is relatively free to increase as the Al–Ti interactions are introduced (Table 5). This distance actually increases to about the same value as found for the edge-sharing case of *M*5 cations. The other relevant factor is that a *M*5 cation shares edges with four other *M*5 cations whereas the *M*4 cation shares a face with only one *M*4 cation. Thus, cation-cation repulsion consideration is far more important for the *M*5 site relative to the *M*4 site. The Ti concentration at the *M*4 site does not exceed 50 %; thus, it is likely that Ti–Ti interactions do not occur at this site, and this may be a factor that limits the Ti substitution into $CaAl_{12}O_{19}$.

5 Supporting information

Final Rietveld fits for all refinements are shown. Relative-permittivity *K* values of $CaAl_{12}O_{19}$, $SrAl_{12}O_{19}$, $PbAl_{12}O_{19}$ and $CaAl_{10}TiNiO_{19}$ are also provided in the online version (DOI: 10.1515/znb-2015-0224).

Acknowledgments: This research done at Oregon State University was supported by National Science Foundation grant (DMR – 1508527). The identification of any commercial product or trade name does not imply endorsement or recommendation by the National Institute of Standards and Technology.

References

[1] K. Keil, L. H. Fuchs, *Earth Planet. Sci. Lett.* **1971**, *12*, 184.
[2] R. G. Burns, V. M. Burns, *J. Geophys. Res. B* **1984**, *89 (Suppl.)*, C313.
[3] M. Nagashima, T. Armbruster, T. Hainschwang, *Miner. Mag.* **2010**, *74*, 871.
[4] K. Kimura, M. Ohgaki, K. Tanaka, H. Morikawa, F. Marumo, *J. Solid State Chem.* **1990**, *87*, 186.

[5] J. J. Comer, W. J. Croft, M. Kestigian, J. R. Carter, *Mater. Res. Bull*. **1967**, *2*, 293.
[6] T. R. Wagner, *J. Solid State Chem*. **1998**, *136*, 120.
[7] X. Obradors, A. Collomb, M. Pernet, D. Samaras, J. C. Joubert, *J. Solid State Chem*. **1985**, *56*, 171.
[8] L.-S. Du, J. F. Stebbins, *J. Phys. Chem. B* **2004**, *108*, 3681.
[9] K. Harindranath, K. A. Viswanath, C. V. Chandranb, T. Bräuniger, P. K. Madhuc, T. G. Ajithkumar, P. A. Joy, *Solid State Commun*. **2010**, *150*, 262.
[10] T. R. Wagner, M. O'Keeffe, *J. Solid State Chem*. **1988**, *73*, 211.
[11] C. A. Geiger, O. J. Kleppa, B. O. Mysen, J. M. Laitimer, L. Grossman, *Geochim. Cosmo. Acta* **1988** *52*, 1729.
[12] D. Saber, A. M. Lejus, *Mater. Res. Bull*. **1981**, *16*, 1325.
[13] M. Gasperin, M. C. Saine, A. Kahn, F. Laville, A. M. Lejus, *J. Solid State Chem*. **1984**, *54*, 61.
[14] N. Iyi, Z. Inoue, S. Takekawa, S. Kimura, *J. Solid State Chem*. **1984**, *54*, 70.
[15] A. Kahn, A. M. Lejus, M. Madsac, J. Théry, D. Vivien, J. C. Bernier, *J. Appl. Phys*. **1981**, *52*, 6864.
[16] F. Laville, M. Perrin, A. M. Lejus, M. Gasperin, R. Moncorge, D. Vivien, *J. Solid State Chem*. **1986**, *65*, 301.
[17] H. H. Mao, M. Hillert, M. Selleby, B. Sundman, *J. Amer. Cer. Soc*. **2006**, *89*, 298.
[18] E. Kreber, U. Gonser, A. Trauiwein, F. E. Harris *J. Phys. Chem. Solids* **1975**, *36*, 265.
[19] A. E. Smith, H, Mizoguchi, K. Delaney, N. A. Spaldin, A. W. Sleight, M. A. Subramanian, *J. Am. Chem. Soc*. **2009**, *131*, 17084.
[20] H. Mizoguchi, A. W. Sleight, M. A. Subramanian, *Inorg. Chem*. **2011**, *50*, 10.
[21] P. Jiang, J. Li, A. W. Sleight, M. A. Subramanian, *Inorg. Chem*. **2011**, *50*, 5858.
[22] A. C. Larson, R. B. Von Dreele, General Structure Analysis System (GSAS); Report LAUR 86-748; Los Alamos National Laboratory, Los Almos, NM, **1994**.
[23] B. H. Toby, *J. Appl. Crystallogr*. **2001**, *34*, 210.
[24] V. Petříček, M. Dušek, L. Palatinus, *Z. Kristallogr. – Cryst. Mater*. **2014**, *229*, 345.
[25] M. O'Keeffe, Eutax; http://ww1.iucr.org/sincris-top/logiciel/prg-eutax.html (accessed February 2016).
[26] K. Kihara, G. Donnay, *Canad. Miner*. **1985**, *23*, 647654.
[27] N. Iyi, M. Göbbels, *J. Solid State Chem*. **1996**, *122*, 46.
[28] W. M. Meier, H. Villiger, *Z. Kristallogr*. **1969**, *129*, 411.
[29] S. Sanna, W. G. Schmidt, *IEEE Trans. Ultra. Ferroelec. Freq. Cont*. **2012** *59*, 1925.
[30] N. Iyi, S. Takekawa, S. Kimura, *J. Solid State Chem*. **1990**, *85*, 318.
[31] H. Graetsch, W. Gebert, *Z. Kristallogr*. **1994**, *209*, 338.
[32] E. Sawaguchi, H. Maniwa, S. Hoshino, *Phys. Rev*. **1951**, *83*, 1078.
[33] E. Sawaguchi, G. Shirane, Y. Takagi, *J. Phys. Soc. Jpn*. **1951**, *6*, 333.
[34] A. W. Sleight, *Prog. Solid State Chem*. **2009**, *37*, 251.
[35] M. E. Lines, *Phys. Rev. B* **1977**, *15*, 388.
[36] Y. Xu, J. D. Mackenzie, *J. Non-Crys. Solids* **1999**, *246*, 136.
[37] G.-L. Tan, M. Wang, *J. Electrocer*. **2011**, *26*, 170.
[38] K. Ebnabbasi, M. Mohebbi, C. Vittoria, *J. Appl. Phys*. **2013**, *113*, 17C703.
[39] L. Wang, D. Wang, Q. Cao, Y. Zheng, H. Xuan, J. Gao, Y. Du, *Sci. Rep*. **2012**, *2*, 223.
[40] K. Ebnabbasi, C. Vittoria, A. Widom, *Phys. Rev. B* **2012**, *86*, 024430.
[41] K. Ebnabbasi, Y. Chen, A. Geiler, V. Harris, C. Vittoria, *J. Appl. Phys*. **2012**, *111*, 07C719.
[42] K. Ebnabbasi, M. Mohebbi, C. Vittoria, *Appl. Phys. Lett*. **2012**, *101*, 062406.
[43] S. Ishiwata, Y. Taguchi, H. Murakawa, Y. Onose, Y. Tokura, *Science* **2008**, *319*, 1643.
[44] S. Ishiwata, Y. Taguchi, Y. Tokunaga, H. Murakawa, Y. Onose, Y. Tokura, *Phys. Rev. B* **2009**, *79*, 180408(R).
[45] S. H. Chun, Y. S. Chai, D. Jaiswal-Nagar, S. Y. Haam, I. Kim, *Phys. Rev. Lett*. **2010**, *104*, 037204.
[46] Y. Kitagawa, Y. Hiraoka, T. Honda, T. Ishikura, H. Nakamura, T. Kimura, *Nat. Mater*. **2010**, *9*, 797.
[47] K. Okumura, T. Ishikura, M. Soda, T. Asaka, H. Nakamura, Y. Wakabayashi, T. Kimura, *Appl. Phys. Lett*. **2011**, *98*, 212504.
[48] Y. Tokunaga, Y. Kaneko, D. Okuyama, S. Ishiwata, T. Arima, S. Wakimoto, K. Kakurai, Y. Taguchi, Y. Tokura, *Phys. Rev. Lett*. **2010**, *105*, 257201.
[49] M. J. Iqbal, M. N. Ashiq, P. H, Gomez, J. M. Munoz, *J. Magn. Magn. Mater*. **2008**, *320*, 881.
[50] E. H. Na, J. H. Lee, S. J. Ahn, K. P. Hong, Y. M. Koo, H. M. Jang, *J. Magn. Magn. Mater*. **2012**, *324*, 2866.
[51] S. Utsumi, D. Yoshida, N. Momozawa, *J. Phys. Soc. Jpn*. **2007**, *76*, 034704.
[52] T. Kimura, G. Lawes, A. P. Ramirez: *Phys. Rev. Lett*. **2005**, *94*, 137201.
[53] T. Kimura, T. Goto, H. Shintani, K. Ishizaka, T. Arima, Y. Tokura, *Nature* **2003**, *426*, 55.
[54] E. H. Na, S. Song, Y.-M. Koo, H. M. Jang, *Acta Mater*. **2013**, *61*, 7705.
[55] M. Magione, M. A. Subramanian, *Appl. Phys. Lett*. **2008**, *93*, 032902.
[56] P. M. Doyle, P. F. Schofield, A. J. Berry, A. M. Walker, K. S. Knight, *Amer. Mineral*. **99**, *201*, 1369.

Supplemental Material: The online version of this article (DOI: 10.1515/znb-2015-0224) offers supplementary material, available to authorized users.